In-cylinder flow control in a four-valve spark ignition engine: numerical and experimental steady rig tests

D Ramajo*, **A Zanotti,** and **N Nigro**
International Center for Computational Methods in Engineering (CIMEC), Güemes, Santa Fe, Argentina

The manuscript was received on 5 May 2010 and was accepted after revision for publication on 21 January 2011.

DOI: 10.1177/0954407011400153

Abstract: Computational fluid dynamic (CFD) simulations and experimental steady flow tests (flow discharge, swirl, and tumble) were carried out to study the in-cylinder flow in a commercial four-valve spark ignition engine. The present investigation was aimed at analysing and controlling the generation of macro-vortex structures (swirl and tumble) during the inlet process. A comparative study of the most commonly employed tumble benches along with in-house design was performed, the last showing some advantages with respect to the others. The outcomes from the simulations were in agreement with experimental results. Mainly, the tumble generation rate was in general proportional to the valve lift. However, tumble was reduced drastically at medium valve lift due to a change in the vortex pattern. A stagnation zone was observed between inlet valves. CFD calculations successfully captured this tumble-fall effect, which was related to characteristic changes in the vortex pattern downstream of the inlet valves at medium valve lift. This affects tumble production without affecting the mass flowrate efficiency. Finally, at high valve lifts the tumble production and the vortex pattern were recovered. The capability of the cylinder head to induce swirl, tumble, or combined swirl–tumble by modifying the valve timing or by introducing adjustable flow deflectors was evaluated using CFD. Several valve timing strategies were analysed: some of them produced significant swirl, but introduced high mass flowrate losses. On the other hand, adjustable flow deflectors were shown to be an interesting alternative to induce swirl–tumble at low load and to improve tumble at high load.

Keywords: steady rig tests, tumble, swirl, computational fluid dynamics (CFD)

1 INTRODUCTION

In-cylinder charge motion has been steadily gaining importance since the introduction of new technologies such as gasoline direct injection or homogeneous charge compression ignition. Understanding the dynamics of the in-cylinder flow structures is the first step to control fuel stratification, turbulence, and heat transfer efficiently. These factors play a crucial role in fuel economy, emissions, and engine performance.

**Corresponding author: International Center for Computational Methods in Engineering (CIMEC), Güemes 3450 (S3000GLN), Santa Fe, Argentina.*
email: dramajo@santafe-conicet.gov.ar

Since the beginning of engine development, experimental tests have been employed to study, design, and improve thermal machines. Owing to the complexity of conducting experimental dynamic tests reproducing real engine operation, several simple steady tests were adopted for engine performance evaluation purposes. One of them is the well-known flow rig test to quantify the mass flowrate (MFR) entering or leaving the cylinder for a given pressure drop. This test allows the estimation of cylinder head aspiration capacity. Moreover, assessment of constructive changes on the cylinder head and inlet ducts can be accomplished with this test. This, in turn, can be used to improve MFR. However, enhancing the steady flow coefficients does not always have a positive impact on engine performance.

As is generally known, the generation of coherent macro-vortex structures (swirl, tumble, or swirl–tumble) is one of the more promising methods to achieve turbulence close to the ignition time, because a well-defined single vortical structure is more stable than other large-scale in-cylinder flows [**1**]. The use of ports promoting tumble increases the initial flame while the moderate tumble and swirl generated by a swirl control valve improves initial flame development coupled with flame convection [**2**].

Swirl and tumble steady rig tests are an easy implementation and a low-cost option to estimate the ability of the cylinder head to convert the linear motion of the inlet flow to rotational motion. For these reasons, such tests are currently used to estimate the effect of geometric changes on the cylinder head and the inlet port with the aim of comparing and improving engine performance. However, steady rig test conditions are far from the real ones, and, therefore, these results should not be used to predict dynamic engine performance [**3**]. On the other hand, some techniques like particle image velocity, laser Doppler anemometry, or the intensified charge-coupled device (ICCD) camera are currently employed to study in-cylinder flow under dynamic conditions [**1**, **2**]. However, in contrast to steady rig tests, dynamic tests are extremely complex, laborious, and expensive. Thus, steady rig tests have been extensively employed, sometimes combining computational fluid dynamics (CFD) and experimental results, thereby allowing for a better understanding of the in-cylinder flow [**4**–**9**].

The development of CFD methodology and computer codes for engine simulation has been a challenging task during the last four decades since the introduction of KIVA code [**10**]. Reciprocating engines exhibit many complex features and physical phenomena. On the one hand, there is geometrical complexity, because of the shapes of the combustion chamber, piston crown, and inlet and exhaust ports, along with the valve and piston motion [**7**, **11**]. On the other hand, there are many simultaneous interacting thermofluids processes, including: non-stationary turbulent flow, heat and mass transfer, injection, atomization, dispersion and evaporation of liquid fuel, and ignition and combustion of the charge. These features place stringent demands on the two core areas of CFD; namely mathematical modelling and numerical solution methodology.

On the modelling side, the task is to assemble a suitable, accurate, and economical mathematical description of the aforementioned physical processes. As is well known, to meet these requirements it is necessary to introduce approximations, such as the Reynolds averaging approach to turbulence or reduction of complex chemical kinetics mechanisms to simpler forms.

The task for the numerical analyst is to assemble an algorithm for solving the model equations in a flexible, accurate, economical, and speedy fashion. While the flexibility requirement is associated with the geometry-handling capabilities, the remaining numerical requirements are determined by the discretization accuracy, solver efficiency, and computer implementation, lately improved by the availability of parallel computers.

Substantial advances have been made in all the aforementioned areas, particularly during the past decade, such that CFD simulation now has reasonable credibility within the engine community. However, there are additional requirements to be met for it to become a design tool: mainly an easy-to-use methodology to spread the work widely within the engineering community, and including rapid mesh generation, short simulation time, and appropriate data visualization/analysis tools.

Finally, a perhaps less obvious challenge to CFD simulation is the limited availability of suitable experimental data to guide the development and assess the accuracy of the methodology. In recent works [**3**, **8**] CFD was applied to study a four-valve-per-cylinder Fiat engine. Dynamic hot engine simulations of the whole engine were compared with steady-state cold simulations in order to identify differences in in-cylinder flow. Tumble generation was also studied in depth for both cases.

The goal of the present work is to use CFD to assess different tumble benches (termed ACT) currently employed for steady rig tests. Some aspects of the in-cylinder vortex structures are also clarified. CFD and experimental flow discharge tests, tumble tests, and swirl tests are carried out. Finally, different strategies, like valve timing and inlet-flow deflectors, are evaluated with a view to control and enhance the swirl and tumble production.

Since this research was implemented on a typical and commonly employed cylinder head (four-valve pentroof chamber) of a commercial four-cylinder Fiat Torque engine, the conclusions from this work can be applied to a large number of engines.

2 METHODOLOGY

In general, steady test configurations are not standardized. A whole range of measurement devices, techniques, and test conditions are employed. For this reason, it is important to report not only the

Table 1 Engine data

Cylinders:		
Fuel	Gasoline	
Number of cylinders	4	
Piston displacement	395.5 cm^3	
Bore	87 mm	
Stroke	68 mm	
Compression ratio	10.5:1	
Connecting rod length	118 mm	
Valves:		
	Intake	Exhaust
Diameter	30.4 mm	29.9 mm
Maximum lift	9 mm	8.5 mm
Maximum lift time (CA)	102.5°	618.5°
Opening range	255°	253°
Opening advance	25°	48°
Closing retard	50°	25°

Table 2 Description of the flow rig tests performed in this study

Test	Type of measurement
1	Flow coefficients of the intake system
2	Flow coefficients of the exhaust system
3	*Swirl*. Right valve closed
4	*Swirl*. Right valve delayed 1.51 mm
5	*Tumble*. Both valves equally opened (*MS* in P_2)
6	*Tumble*. Both valves equally opened (*MS* in P_4)
7	*Tumble*. Right valve delayed 1.51 mm (*MS* in P_2)
8	*Tumble*. Left valve kept at 3.03 mm (*MS* in P_4)
9	*Tumble*. Left valve kept at 4.54 mm (*MS* in P_4)
10	*Tumble*. Right valve kept at 4.54 mm (*MS* in P_4)

test results but also the test conditions. Simulations were performed reproducing the experimental conditions. Table 1 shows the main constructive and operative characteristics of the engine. The maximum valve lift analysed in this work was greater than that corresponding to the real engine.

2.1 Experimental test

Three kinds of steady tests were carried out, namely, the flow discharge, swirl, and tumble tests. Experimental tests were performed for the original cylinder head. The incorporation of flow deflectors inside the inlet port was only assessed by CFD. For all the tests the cylinder head was subjected to a constant pressure drop of 25 in of water column, this was accomplished using a flowmeter, SuperFlow SF-600. An accuracy of ± 0.5 per cent and a repeatability of ± 0.1 per cent at full scale are reported for this device. A rotary honeycomb swirl meter (SM) (AUDIE Technology) was employed for angular momentum measurements (swirl and tumble tests). Table 2 summarizes the tests performed.

As regards the flow discharge tests (tests 1 and 2), both the intake and the exhaust systems were studied, considering seven valve lifts in each case. The flow was driven in the same direction as the flow that is naturally induced under dynamic engine conditions. In other words, this means entering the cylinder at the intake system, and leaving the cylinder by the exhaust system. In order to reduce boundary influence and acoustic effects, a cylinder 0.1 m in height was placed between the cylinder head and the flowmeter plenum. Also, a smooth shaped nozzle and a diffuser were found at the beginning and at the end of the intake and the exhaust ports, respectively.

Swirl tests were performed adding the SM below (downstream of) the cylinder. Tumble tests were done with an in-house L-shaped tumble bench design (Fig. 1), which was adopted after a CFD comparative study with the most typical tumble benches. More details are given in section 2.5.

Significant swirl and tumble variation was observed during the tests, indicating the existence of complex vortex dynamics. On the contrary, for flow discharge tests, negligible variations were observed.

2.2 Numerical procedure

Simulations were performed using the commercial volume of fluid package software ANSYS-CFX 10.0. The Navier–Stokes mass and momentum equations (isothermal model) were applied. The mass balance can be expressed as

$$\frac{\partial \rho}{\partial t} + \nabla \cdot (\rho \boldsymbol{U}) = 0 \tag{1}$$

where ρ is the density and $\boldsymbol{U}$ is the Reynolds average velocity. The momentum equation can be expressed as

$$\frac{\partial}{\partial t}(\rho \boldsymbol{U}) + \nabla \cdot (\rho \boldsymbol{U} \otimes \boldsymbol{U}) = -\nabla P + \nabla \cdot \tau + \phi \tag{2}$$

where P is the static pressure, τ is the shear stress tensor, and ϕ is an external volumetric momentum source (potential force fields, i.e. gravity).

Turbulence was modelled through a standard k–ε model, which is commonly employed for performing steady and dynamic engine simulations [**3**, **7**, **12**–**15**]. The transport equations for the turbulent kinetic energy k and the turbulence dissipation rate ε are

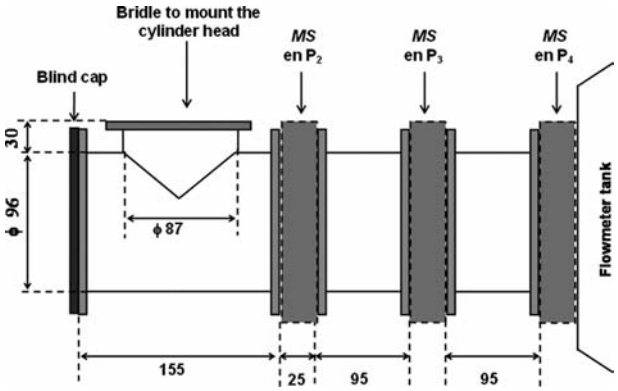

Fig. 1 Sketch of the tumble bench configuration employed to perform the tumble tests

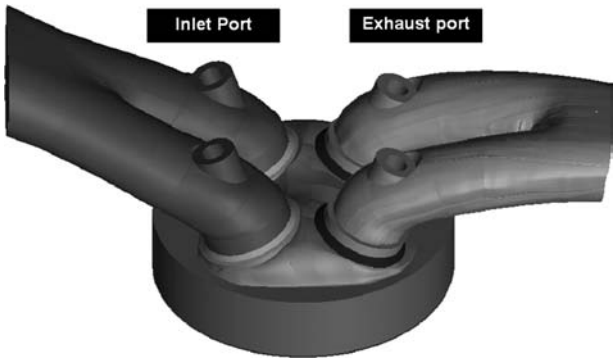

Fig. 2 Computational domain

$$\frac{\partial(\rho k)}{\partial t} + \frac{\partial(\rho U_i k)}{\partial x_i} = \frac{\partial}{\partial x_i}\left(\frac{\mu_t}{\sigma_k}\frac{\partial k}{\partial x_i}\right) + G - \rho\varepsilon$$
$$\frac{\partial(\rho\varepsilon)}{\partial t} + \frac{\partial(\rho U_i \varepsilon)}{\partial x_i} = \frac{\partial}{\partial x_i}\left(\frac{\mu_t}{\sigma_\varepsilon}\frac{\partial \varepsilon}{\partial x_i}\right) + \frac{\varepsilon}{k}(C_1 G - C_2\rho\varepsilon) \quad (3)$$

where μ_t is the turbulent viscosity, which is obtained from the eddy viscosity model

$$\mu_t = \frac{C_\mu \rho k^2}{\varepsilon} \quad (4)$$

C_1, C_2, σ_k, σ_ε, and C_μ are model constants, being 1.44, 1.92, 1.0, 1.3, and 0.09, respectively. In equations (3) and (5), G is a turbulence production term estimated from the velocity gradient and the turbulent viscosity μ_t as

$$G = \frac{1}{2}\mu_t\left(\nabla\bar{U} + (\nabla\bar{U})^T\right)^2 \quad (5)$$

A scalable wall law was employed to model the near-wall flow. As regards the boundary conditions, a total pressure was fixed at inlet (atmospheric pressure), while an opening condition was employed at outlet (it allows flow to leave or enter the domain according to the pressure gradient at the boundary). A smooth no-slip condition was applied at the walls, with the exception of the intake and exhaust port walls, where a roughness of 0.2 mm was applied. Simulations were carried out using distributed calculus in a Beowulf cluster with 20 processors (Intel Pentium IV, 1 Gb RAM).

Positive replicas from the intake and exhaust ducts (using low-contraction silicone) and from the combustion chamber (employing high-rigidity polyester resin) were made in order to measure the cylinder head geometry. Replicas were scanned (three-dimensional rotary laser scanner Roland LPX-250), obtaining the tridimensional position of a large number of points (around 5.5×10^5 points for the overall model). Points were loaded in software GID 7.2 and a set of characteristic path lines were drawn. Lines were exported to ANSYS-ICEM 10.0 to build surfaces, thus obtaining the final model shown in Fig. 2.

The meshes were generated in ANSYS-ICEM 10.0. Around 2×10^6 tetrahedral elements were required to obtain an accurate description of the steady rig bench geometries. The cylinder and the cylinder head (especially around valves) were refined in order to capture the complex characteristics of the flow. Figure 3 displays the computational model corresponding to the swirl rig bench.

2.3 Simulation

The simulations were transient owing to the fact that numerical and experimental results showed pseudo-steady behaviour. In order to avoid overflow problems, the cylinder head was subjected to a pressure drop, which was linearly increased from 0 to a constant value of 25 in of water (the same as in the experimental procedure). Owing to the unsteady nature of the three-dimensional turbulent flows, variations in MFR and angular momentum persisted after the steady-state pressure drop was established. This phenomenon was consistent with what was observed during the experimental tests. Therefore, the steady-state results were obtained by an average of ten solutions, equally spaced in time, within a suitable period of time starting once a pseudo-steady solution was observed. For flow discharge simulations the quasi-steady solution was quickly reached (after 100 time steps). On the other hand, for swirl and tumble simulations more than 1000 time steps had to be simulated. In a similar study the slow evolution of tumble convergence was also reported [**4**].

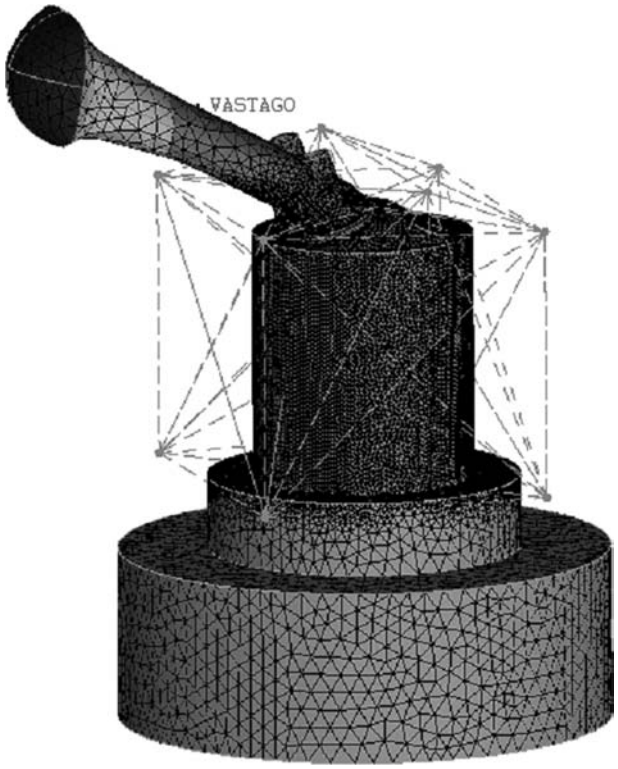

Fig. 3 Surface mesh of the computational model used for steady swirl test simulations

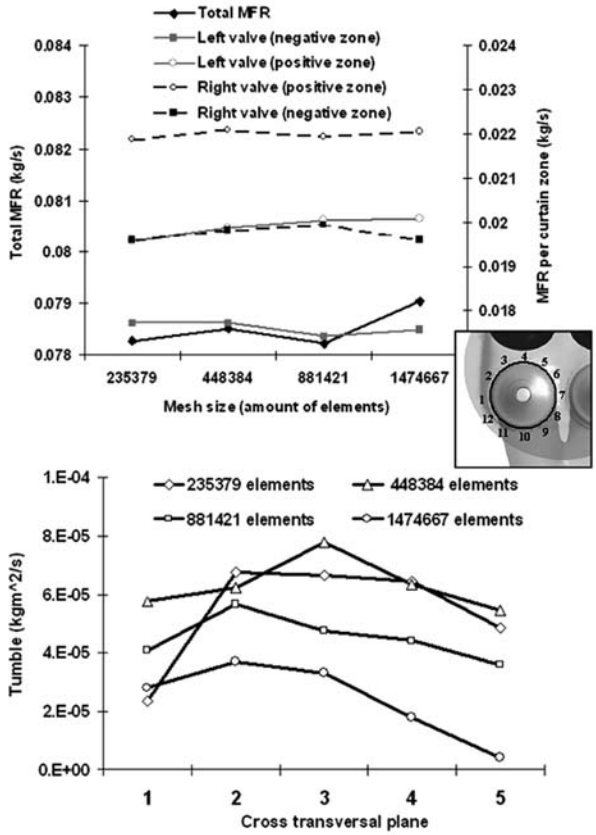

Fig. 4 Mesh convergence. Top: influence on MFR; bottom: influence on tumble production

2.4 Mesh convergence

Mesh convergence was analysed considering several mesh cell sizes and time steps. Figure 4 (top) shows the MFR obtained for four different meshes. The solid black line indicates the total MFR entering the cylinder, while the other four lines were obtained by dividing each one of the two valve curtains into two halves. The positive curtain zones correspond to the half of the curtains from 1 to 7, which are called positive by assuming that the flow entering through these zones produces positive tumble momentum. In Fig. 4 (top) the scale on the left corresponds to the total MFR, while the scale on the right corresponds to the MFR at each zone. A slight variation in MFR can be clearly observed by refining the mesh.

Figure 4 (bottom) shows the tumble momentum generated by the flow through five cross-transversal planes cutting through the cylinder. For the tumble estimation in each plane, the imaginary tumble axis is placed over the corresponding plane. Planes 1 to 5 are located at 10, 30, 50, 70, and 90 mm from the cylinder head, respectively. It should be noted that significant differences are observed for the four meshes. Results from meshes A and B are rather similar, whereas mesh C is closer to the finest one (mesh D), with the curves C and D having a similar behaviour. As a compromise between cost and accuracy, mesh C is used in the rest of this paper for comparative studies, defining an element size of 1.1 mm.

Regarding time step convergence, Fig. 5 shows the results obtained for a time step range from 2×10^{-4} s to 1×10^{-5} s. Both the MFR and the tumble momentum were evaluated. The MFR holds almost constant for all the analysed time steps. However, the effect of the time step over the momentum production can be clearly noted by analysing Fig. 5 (top). From this convergence analysis a time step of 5×10^{-5} s was adopted.

2.5 Tumble bench study

Similarly to the other steady rig tests, there is not a standardized methodology to perform the tumble and swirl rig tests. One important drawback is the possibility of comparing results from different researchers that employ different test procedures. Regarding the tumble test, the problems are even worse because the tumble benches are different from the engine geometry. It is difficult to imagine a tumble bench that will take into account the

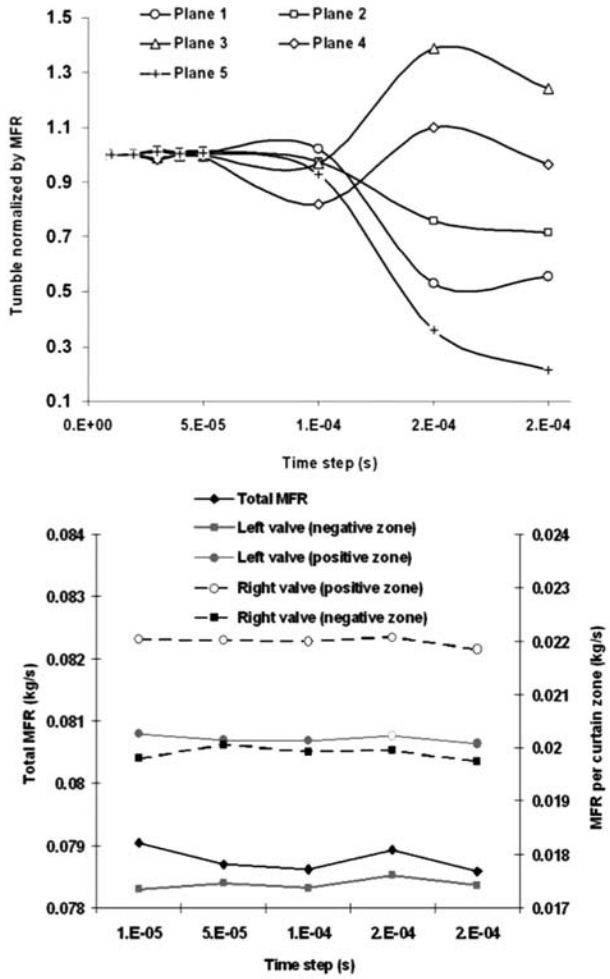

Fig. 5 Time step convergence. Top: influence on MFR; bottom: influence on tumble production

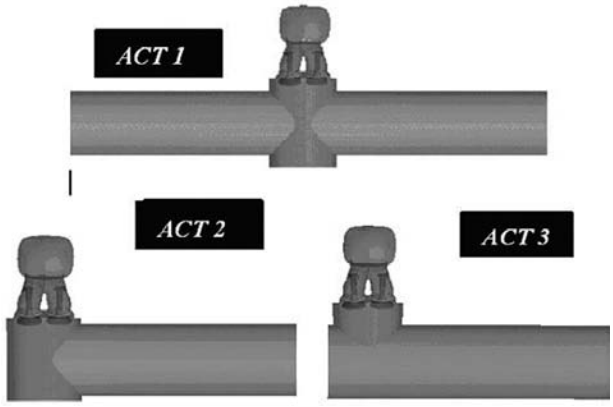

Fig. 6 Tumble bench designs analysed by CFD

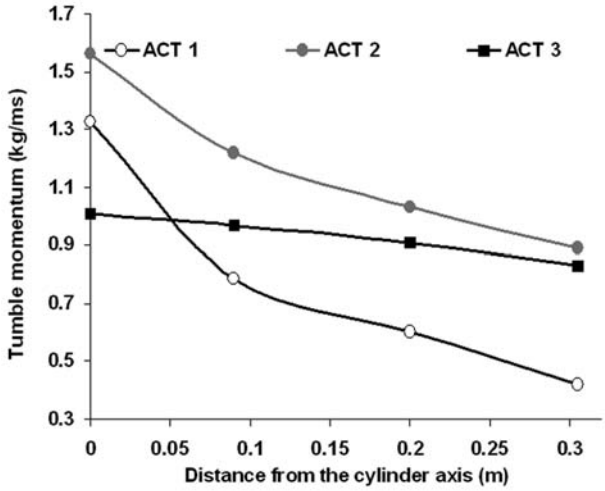

Fig. 7 Tumble momentum obtained from the different tumble benches

whole engine geometry (inlet/outlet ports, valves, combustion chamber shape, cylinder bore and length, and piston crown shape) along with the operation conditions (dynamic pressure variation, piston and valves motion, and thermal effects). An interesting discussion on this subject can be found in reference [**16**].

In the present work three tumble bench designs (see Fig. 6) were assessed by CFD in order to find which one best represents the in-cylinder tumble pattern. ACT 1 and ACT 2 correspond to commercial designs, while the last (ACT 3) is an in-house design. Model ACT 1 is denominated by a T-shaped tumble bench, having two lateral ducts for flow discharging. The other two models are denominated by L-shaped tumble bench. For ACT 1 and ACT 2 the lateral duct has the same diameter as the cylinder bore. On the other hand, for the proposed model, the lateral duct diameter is 10 per cent larger than the cylinder bore.

The tumble loss rate along the lateral duct was evaluated for the three models. Figure 7 shows the results obtained at the cylinder position (P_1) and at three locations along the lateral duct for the maximum valve lift (10.60 mm). ACT 1 and ACT 2 showed a local tumble reduction between positions P_1 and P_2, probably caused at the joint between the cylinder and the lateral duct. As can be seen, ACT 1 and ACT 2 showed the same tumble loss rate between locations P_2 and P_4. On the other hand, ACT 3 showed negligible tumble loss between P_1 and P_2 and the smallest tumble loss rate along the lateral duct (from P_2 to P_4). For these reasons the ACT is the more suitable tumble bench for performing tests.

The proposed tumble bench (ACT 3) has some interesting characteristics: first, the tumble loss rate

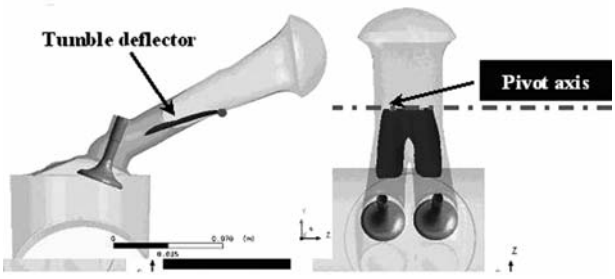

Fig. 8 Views of one tumble deflector (TD_2)

along the lateral duct is almost linear and is small because of the larger duct diameter. Second, the local angular momentum loss at the joint between the cylinder and the lateral duct is negligible, allowing the in-cylinder tumble estimation by linear extrapolation from two measures along the lateral duct. Finally, the L-shaped configuration is not symmetric with respect to the cylinder mean plane. However, for the ACT 3 configuration there is no significant difference in the tumble induced by one of the intake valves when the other valve is kept closed. This means that the valves produce the same tumble regardless of which one is the closest to the lateral duct.

2.6 Incorporation of flow deflectors

The introduction of two kinds of adjustable deflectors inside the inlet ports was evaluated by CFD. While one deflector is included for tumble enhancement, the other is introduced for swirl production. These deflectors were designed to be mounted together inside the inlet ports, adopting different positions to control the inlet flow according to the engine requirements.

Three tumble deflectors (TDs) were studied. They were built by offsetting a portion of the bottom surface of the inlet duct, differing in length (35 mm for TD_1, 50 mm for TD_2, and 70 mm for TD_3). Figure 8 displays the TD_2. TD rotation was allowed around a pivot axis, testing several TD positions. Owing to the high computational cost of simulations only one valve lift (10.6 mm) was considered in a preliminary study. Then, the most efficient TDs were studied in depth.

Regarding swirl generation, only one swirl deflector (SD) design was analysed. Figure 9 shows a view of it. Also in this case the SD was allowed to rotate around a pivot axis to partially obstruct one of the inlet valves. Five positions and a unique valve lift (10.6 mm) were considered for the SD.

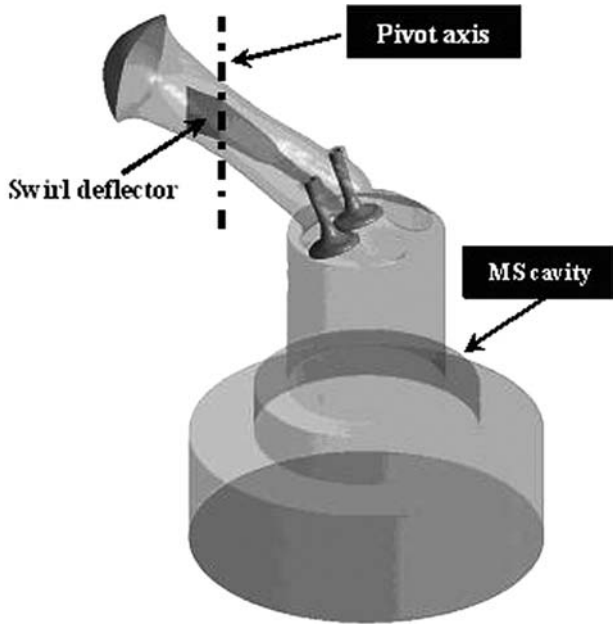

Fig. 9 View of the swirl deflector (SD)

3 RESULTS AND DISCUSSION

3.1 Steady flow tests

Figure 10 shows the results for flow coefficients C_D and C_f for the intake and exhaust systems. Agreement between CFD and experimental results can be observed. Differences between numerical and experimental results become larger at mean valve lifts, with the averaged relative error closer to 6.5 per cent, while the maximum relative error reaches 10 per cent. As noted, both the discharge (C_D) and the flow (C_f) coefficients are drawn. Owing to the fact that the former considers the valve curtain area, it is more sensitive at low valve lift. On the contrary, the C_f considers the constant cross-sectional area of the valve seat, reflecting the behaviour of the overall port for high valve lift [**16**].

A comparison of the flow coefficients (C_f) for the inlet and exhaust systems shows that the last has a better efficiency at low valve lifts (below 4.5 mm) while the former becomes 17 per cent more efficient at the maximum valve lift. As reported in Table 1, the real maximum valve lifts of the engine are 9 mm and 8.5 mm for the intake and exhaust systems, respectively. This real valve timing seems to be appropriate due to the fact that the MFR is increased only 2.5 per cent by increasing the intake valve lift from 9.09 mm to 10.6 mm. Moreover, the increment for the exhaust system is less than 1 per cent.

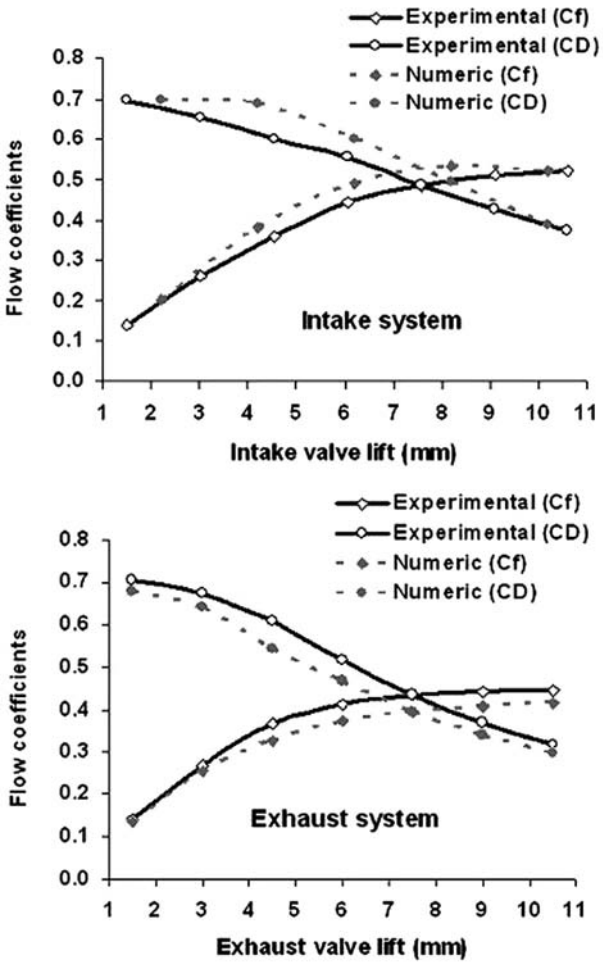

Fig. 10 Flow coefficients (C_D and C_f) for the intake (top) and the exhaust (bottom) systems

3.2 Swirl tests

As expected, four-valve cylinder engines induce negligible swirl motion. In this sense, two intake-valve timings were explored in order to know the potential of the cylinder head to produce swirl.

1. Test 3: one valve completely closed and the other one completely opened.
2. Test 4: one valve partially opened (delayed 1.51 mm with respect to the other) and the other one completely opened.

In order to compare numerical and experimental results, the measured angular velocity ω (1/s) from the MS was converted to volume-averaged angular momentum (kg/m s) by assuming rigid solid rotation for the fluid. That is, the tangential velocity V_t at any point was computed as the product $\omega \times r$, with r being the distance from that point to the cylinder axis. Then, the swirl momentum was obtained from the following expression

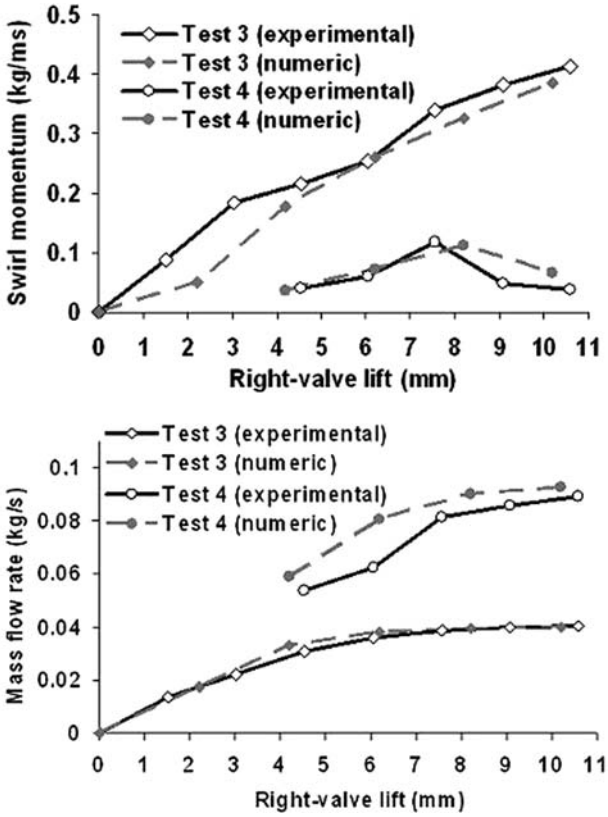

Fig. 11 Numerical and experimental results from swirl tests. Top: swirl momentum; bottom: mass flowrate

$$M_s = \int_{vol} \rho V_t r \, dV = \int_0^R 2\pi r l \rho r \omega r \, dr$$

$$= 2\pi l \rho \omega \int_0^R r^3 \, dr = \pi l \rho \omega \frac{Bo^4}{32} \quad (6)$$

where Bo is the cylinder bore, l is the cylinder height (0.1 m), and ρ is the fluid density.

It is important to point out that the use of the SM did not introduce a noticeable pressure drop during the experimental swirl tests. A comparison of the results obtained with and without the SM showed a maximum MFR reduction of only 0.4 per cent at the maximum valve lift (10.6 mm). Moreover, the fact that the honeycomb of the SM rotates with the flow made it possible to neglect its effect over the flow. Then, only the SM cavity was included in the computational model (see Fig. 9).

Numerical and experimental swirl results are shown in Fig. 11 for both valve timings (test 3 and test 4). It can be seen that numerical results are in agreement with the experiment, but differences in MFR increase for test 4. As noted on the top plot of Fig. 11, swirl generation is almost linear when

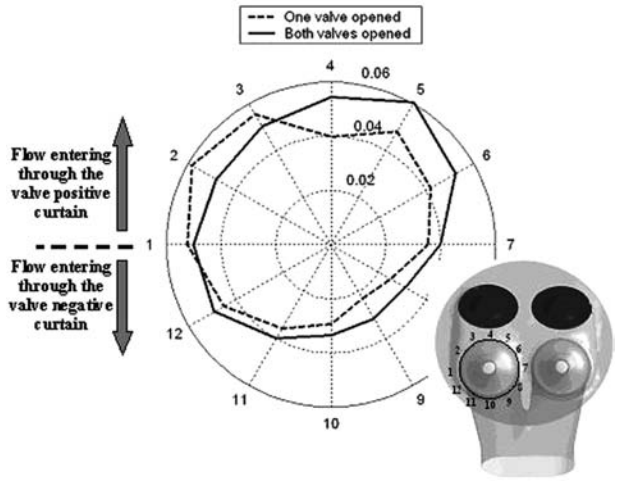

Fig. 12 MFR distribution around the valve curtain by opening both valves and only one of them

only one valve is opened (test 3), even though for mean and high valve lift the MFR keeps almost constant, as noted from Fig. 11 (bottom). From these results, the linear increment of swirl along the valve lift range cannot only be related to the increase in MFR, but also to changes in the flow distribution around the valve curtain.

Analysing the remaining valve timing considered (test 4), the valve-lift delay induces small amounts of swirl at medium valve lifts. However, at high valve lift (at the beginning of the asymptotic MFR behaviour) the MFR through both valves becomes nearly similar and swirl production drops. In this sense, Grimaldi *et al.* [**17**] found similar results by experimental steady tests. Mahrous *et al.* [**14**] performed dynamic simulations, finding that in order to induce significant swirl the valve-lift delay had to be higher than 100 per cent.

Figure 12 shows the MFR distribution around one of the valve curtains at the maximum valve lift (10.6 mm). Note that, if only one valve is opened (test 3) the flow is directed towards the 1–3 direction, clearly influenced by the intake duct. On the other hand, when both valves are equally opened (flow rig test 1) the flow is directed towards the central zone between valves, that is, towards the 4–6 direction. Similar results have been reported by other researchers [**5**, **7**].

3.3 Tumble tests

Figure 13 shows numerical and experimental results obtained by evaluating the tumble at two positions, P_2 and P_4, along the lateral duct of the tumble bench (corresponding to tests 5 and 6, respectively). Numerical results of in-cylinder tumble are also

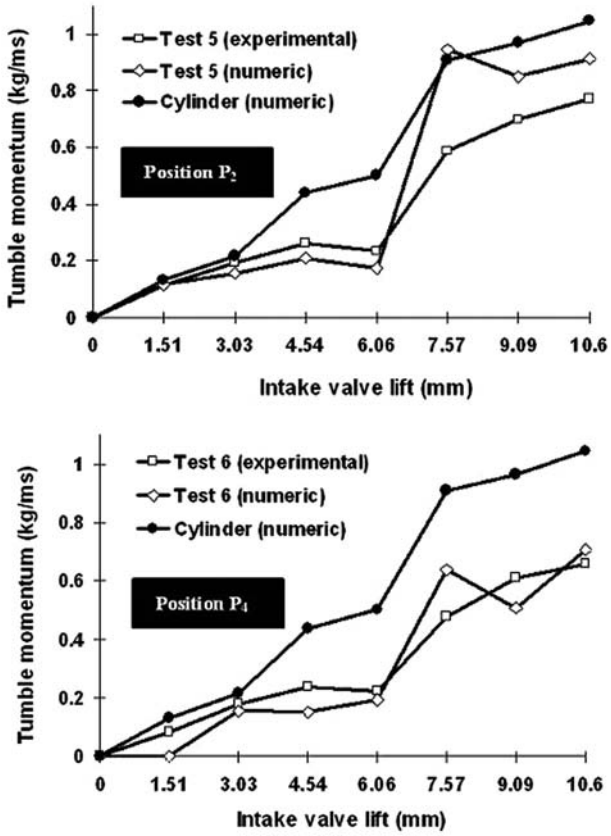

Fig. 13 Numerical and experimental tumble results at two positions along the lateral duct of the ACT. Top: at P_2 position; bottom: at P_4 position

included. A good agreement is found at low valve lifts at P_2 and P_4 positions. However, at position P_2 (Fig. 13, top) tumble is strongly overestimated at high valve lifts, with the maximum relative error closer to 61 per cent (at 7.57 mm), while the average relative error reaches 25 per cent. At position P_4 the maximum relative error reaches 32 per cent (at 7.57 mm), but the average relative error increases to 32 per cent. Numerical and experimental results differ noticeably. However, similar studies arrived at differences higher than 100 per cent [**5**, **6**]. The tumble-fall effect at medium valve lift is well predicted by CFD, being less noticeable inside the cylinder than inside the lateral duct.

When comparing the experimental results at P_2 and P_4 positions, both curves show a similar behaviour, indicating that the tumble loss rate along the lateral duct is nearly linear, being 14 per cent at the maximum valve lift (10.6 mm). As expected, the tumble bench introduces an additional pressure drop evidenced by a reduction of 7 per cent in the MFR at the maximum valve lift. By tracing a straight line connecting the first and the last point of each

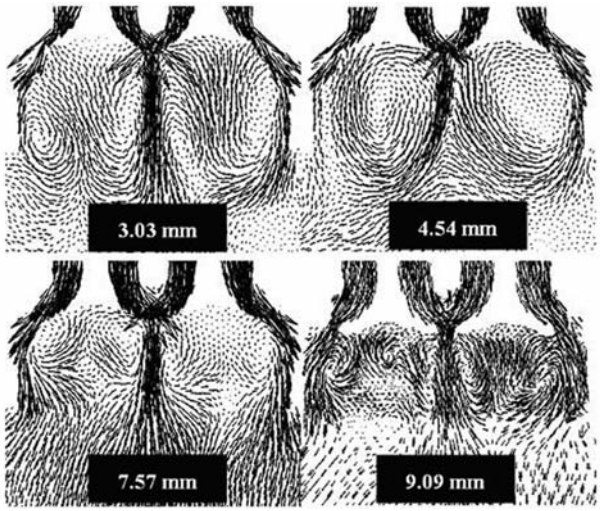

Fig. 14 Velocity pattern below the intake valves for several valve lifts

tumble curve in Fig. 13, it can be noted that tumble generation is nearly proportional to the valve lift, except where the tumble-fall effect takes place.

As shown in Fig. 14, significant changes in the velocity pattern below the intake valves appear as valve lift increases. The velocity pattern at 3.03 mm is characterized by four small vortices, one at each side of the valves. Vortices rotate promoting flow entrance around the whole valve, especially through the zone between valves. For mean valve lifts (around 4.54 mm) only two large vortices can be identified, both having the same rotating sense. The left vortex promotes the flow entrance through the zone between valves, while the other one obstructs the flow in this zone. Finally, after 7.57 mm valve lift the velocity pattern becomes similar to that observed at low valve lift.

Figure 15 (top) shows experimental tumble and MFR results obtained at positions P_2 and P_4. As noted, both curves show the same behaviour and differences in results can be associated with the tumble loss along the lateral duct. Evidently, tumble generation strongly falls at mean valve lift, quickly recovering the production rate at high valve lift. This typical behaviour can be mitigated by changing the valve timing, for example delaying one valve with respect to the other. Figure 15 (bottom) compares the effect of introducing a small delay of 1.51 mm between valves. Note that the tumble fall is reduced, but tumble at high valve lift also decreases. Moreover, a significant reduction of the volumetric efficiency at mean valve lift is found.

The MFR around the valve curtains for tumble tests (valves equally opened) is shown in Fig. 16. As noted, for low and mean valve lift (less than

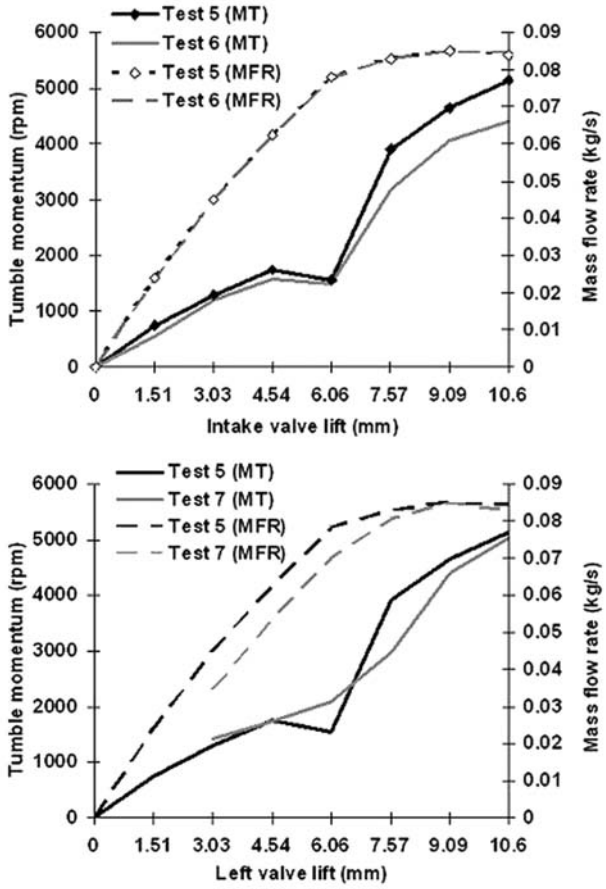

Fig. 15 Experimental results for tumble momentum and MFR. Top: tests 5 and 6; bottom: tests 5 and 7

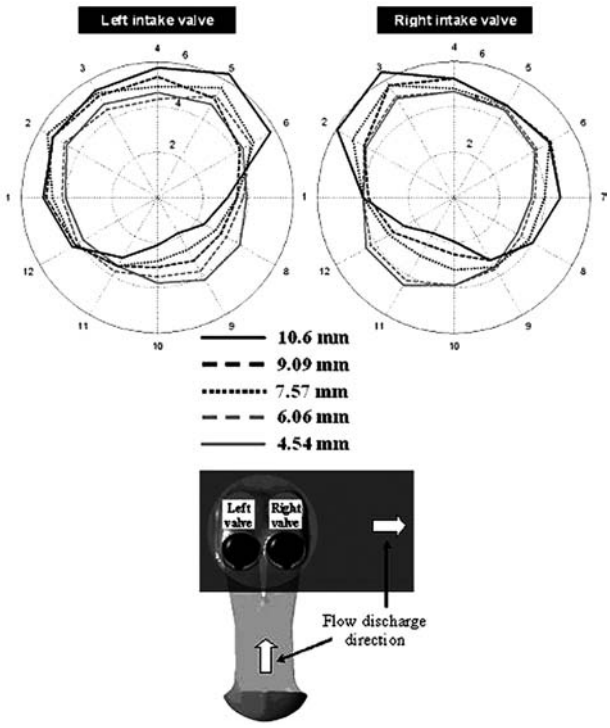

Fig. 16 MFR distribution around the valve curtains

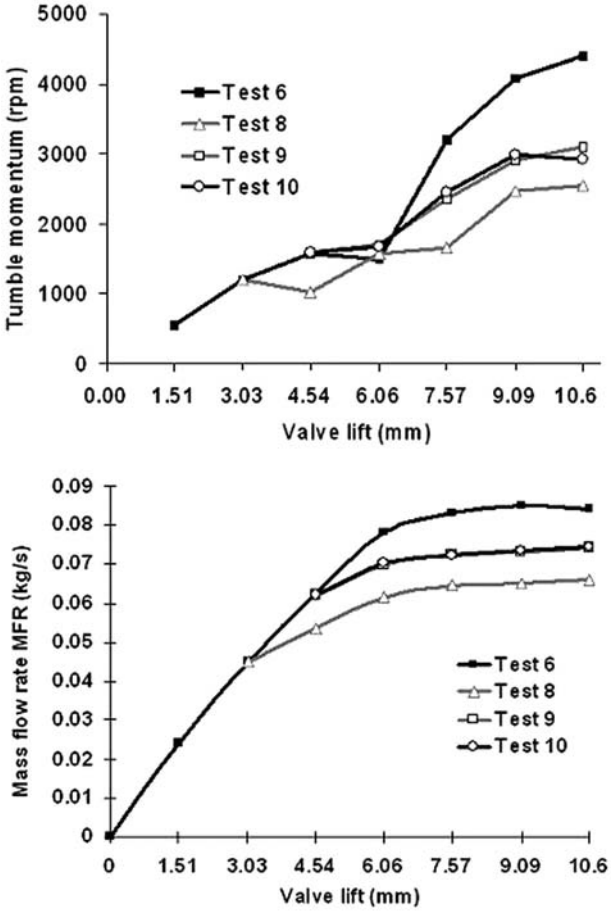

Fig. 17 Experimental results from tests 6, 8, 9 and 10. Top: tumble momentum (r/min); bottom: MFR

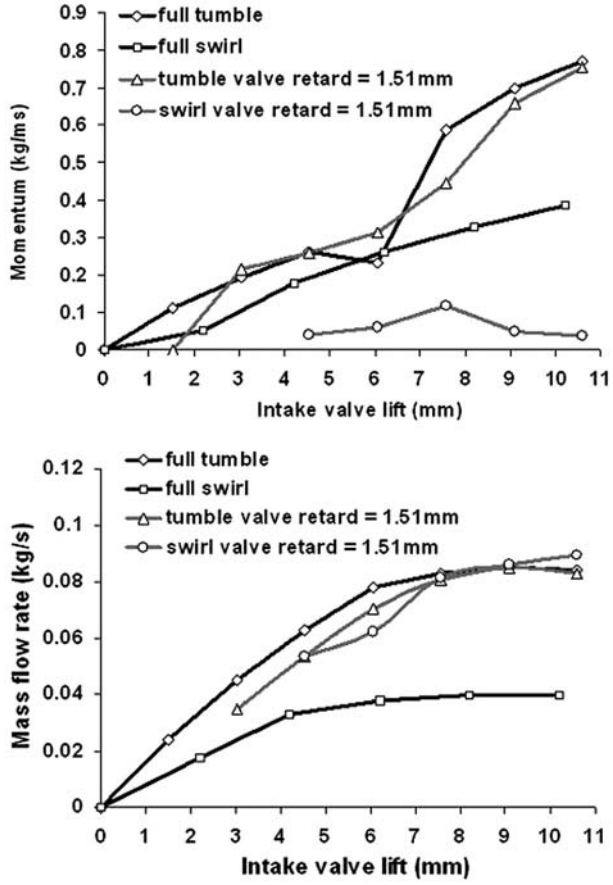

Fig. 18 Four strategies to generate in-cylinder angular momentum (swirl or tumble). Top: angular momentum values; bottom: MFR

6.06 mm) the flow follows the direction given by the intake ducts. But, when the valve lift is increased, the flow progressively turns toward the zone between valves.

Figure 17 displays the experimental results of tumble tests obtained when one valve is kept at a constant position while the other valve is opened. As noted from test 8 (left valve is kept at 3.03 mm), tumble evolution is rather erratic. Moreover, the tumble and the MFR are clearly reduced with respect to the test 6 results (both valves are equally opened). Figure 17 also depicts the results obtained by keeping the left valve (test 9) or the right valve (test 10) opened at a constant position (4.54 mm). As previously mentioned, the tumble bench used (ACT 3) is not symmetrical with respect to the mean plane of the cylinder. However, by comparing tests 9 and 10, any one of the valves induces almost the same tumble and MFR. This is rather different from the results reported by other researchers, who used L-shaped tumble benches similar to the ACT 2 [**5**, **6**].

The fuel burning rate is directly related to the turbulence intensity [**4**, **18**–**21**], which could be controlled depending on the engine regime. Steady tests are the first step in developing valve timing strategies that allow control of the in-cylinder flow [**5**, **13**, **22**–**25**]. Combined tumble–swirl motion was found to be more effective than pure tumble to produce faster and more stable combustion under lean mixture conditions [**2**]. Figure 18 compares four strategies to induce angular momentum (swirl or tumble) by using different valve timing configurations in order to estimate the intensity of momentum that could be induced by using variable valve lift. Full tumble (valves equally opened) appears to be the most effective form to induce in-cylinder momentum for this engine. This figure makes it possible to estimate the effect produced by a small valve delay of 1.51 mm. Owing to the fact that it is not possible to estimate swirl and tumble simultaneously, swirl results correspond to test 4, whereas tumble results correspond to test 7. The small valve delay smoothes the tumble generation, reducing the tumble-fall. Moreover, little swirl is produced at

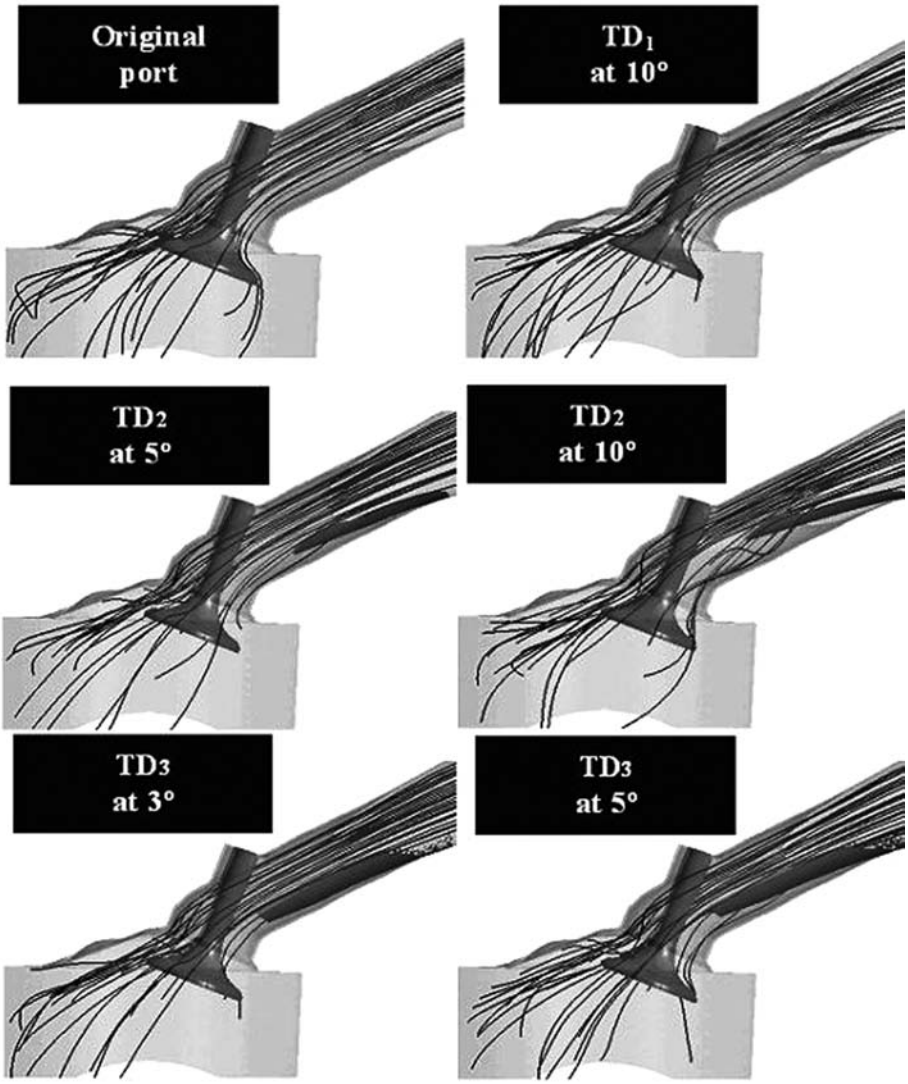

Fig. 19 Streamlines showing the flow deviation introduced by TDs

mean valve lift, also reducing the MFR mainly at low and mean valve lift. On the other hand, if only one valve is opened (full swirl), the momentum production is less than half of that obtained at full tumble and the MFR reduces by more than 50 per cent.

It is clear that the full swirl strategy would not be suitable at high load and high engine speed. The conservation of high tumble from the intake stroke until the end of the compression stroke can be related to the shape and intensity of the macro vortex of tumble [**1**, **15**, **26**]. In this sense, the conservation of swirl motion is promoted by the cylinder shape [**27**]. For this reason, swirl is advantageous at partial load and low engine speed, while tumble is more advantageous at full load and high engine speed. The small valve delay studied (1.51 mm, that is 16 per cent of the maximum valve lift of the real engine) is not enough to produce noticeable significant swirl.

3.4 Geometric modifications: flow deflectors

Small changes inside the inlet ports can produce increments of 100 per cent on swirl or tumble motion, enhancing by more than 20 per cent the turbulent kinetic energy before the ignition [**18**, **28**, **29**]. Moreover, volumetric efficiency is not necessarily reduced. In this sense, adjustable deflectors are an interesting option for enhancing and controlling the charge motion and turbulence at low load [**21**, **30**, **31**].

3.5 Tumble deflectors

Three tumble deflectors were assessed by CFD. Deflectors were generated by offsetting a part of the inlet port surface, differing only in length. Figure 19

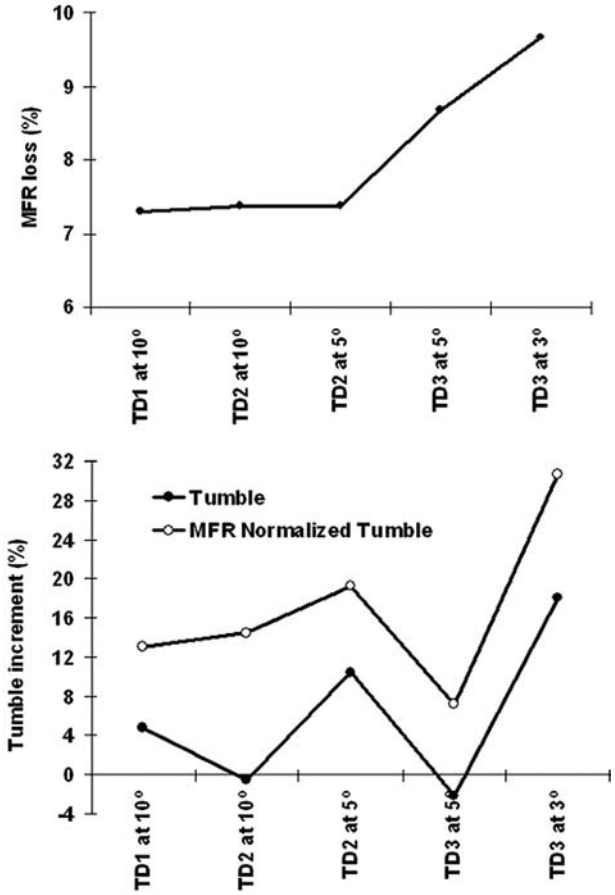

Fig. 20 Results corresponding to 10.6 mm valve lift. Top: percentage of MFR loss. Bottom: percentage of tumble momentum enhancement

shows the streamlines obtained for the original port and for the three TDs. All deflectors reduce the flow entering through the negative valve curtain zone (the half curtain between 7 and 1 in Fig. 12). As noted from the streamlines, an excessive deflector angle can produce instability and detachment of the flow at the end of the deflector (see the panel in Fig. 19 corresponding to TD_2 at 10°).

Figure 20 depicts the MFR reduction and the tumble increment obtained by incorporating the deflectors. As expected, all deflectors reduce volumetric efficiency, the worst being the TD_3 at 3°. As regards tumble, the TD_2 at 10° and the TD_3 at 5° reduced tumble production, while the other configurations showed a tumble profit from 4 per cent to 16 per cent. On the other hand, the tumble/MFR ratio showed a significant increment in all cases, reflecting the fact that all deflectors induced a more coherent macro-vortex flow. In this sense, the best performance was obtained for the TD_3 at 3°, with an MFR loss closer to 10 per cent, a tumble profit closer to 18 per cent, and a tumble/MFR ratio increment of 32 per cent.

The behaviours of deflectors TD_2 at 5° and TD_3 at 3° were evaluated for the whole valve lift range. Figure 21 (top) compares the tumble obtained with and without these deflectors. As noted, the deflectors enhance tumble for all valve lift, this being more significant after 4.54 mm. Moreover, the tumble fall becomes negligible.

Figure 21 (bottom) shows the MFR distribution through the positive and negative zones of one valve curtain. Note that the tumble increment obtained by introducing the deflectors is not related to an increment of MFR through the positive curtain zone but to a reduction on the flow through the negative one. The in-time tumble fluctuations observed during the numerical and experimental tests for the original port disappear with the introduction of the TD_3.

3.6 Swirl deflector

To produce swirl motion an adjustable deflector was added. This deflector partially obstructs one of the inlet port ducts. The swirl deflector was designed in such a way that it could be put together with a TD, allowing control of tumble and swirl simultaneously. Figure 22 shows the streamlines produced by the deflector at two positions (20° and 50°).

Figure 23 (top) displays both the total MFR and the corresponding MFR through each one of the valves. The same figure at the bottom shows the swirl generation as a function of the deflector angle. Results correspond to the maximum valve lift (10.6 mm).

The total MFR is drastically reduced by increasing the deflector angle. After 20° the MFR reduction becomes fairly proportional to the deflector angle, even when the MFR through the clear duct (corresponding to the left valve) keeps almost constant. The swirl generation becomes significant after 20°, reaching a maximum of 0.3 kg/m s at 50°. This value is closer to that obtained by keeping one valve completely closed in test 4. However, the MFR loss is smaller than that obtained in test 4, as can be concluded by comparing Fig. 23 (top) with Fig. 11 (bottom).

4 CONCLUSIONS

In this work numerical and experimental steady tests were performed on a commercial four-valve-per-cylinder spark ignition engine. CFD results were in good agreement with experimental ones, establishing the reliability of the numerical tool for studying in-cylinder flow in depth. Tests shed light on some mean-flow characteristics of the cylinder

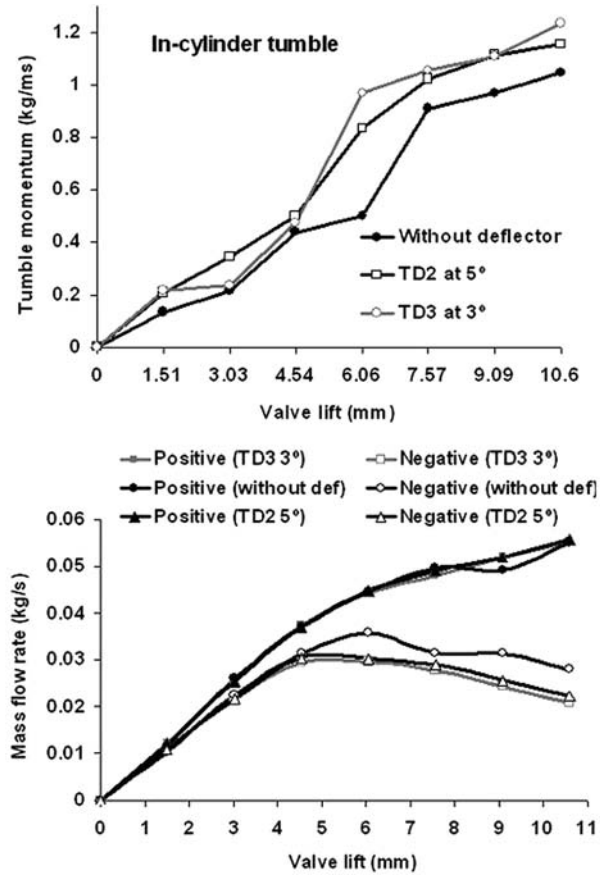

Fig. 21 Top: in-cylinder tumble momentum obtained for the whole valve lift range by using the deflectors TD_2 at 5° and TD_3 at 3°. Bottom: MFR over the positive and negative zones of the valve curtain

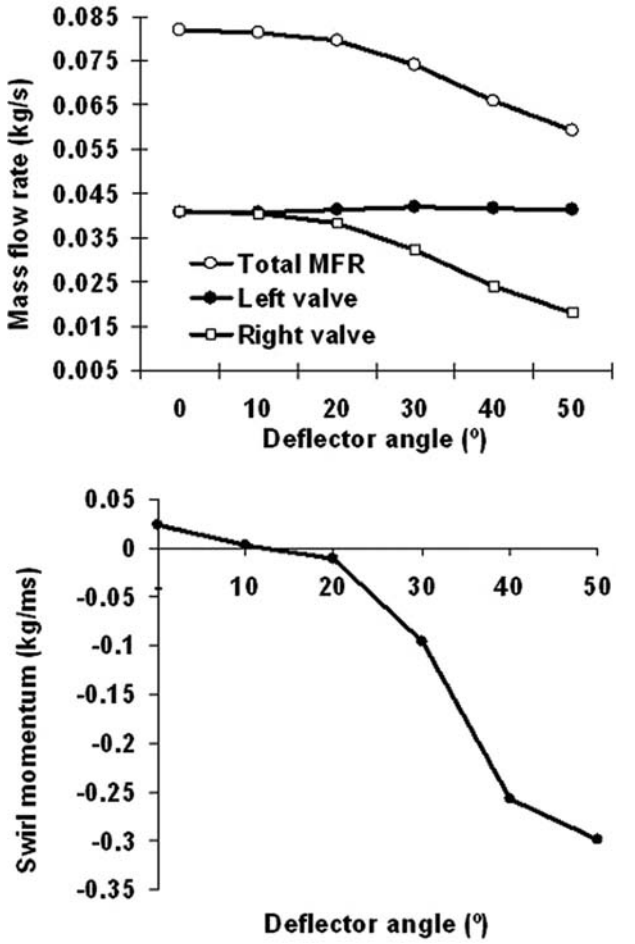

Fig. 23 Top: total and partial MFR as a function of the deflector angle. Bottom: swirl generation as a function of the deflector angle

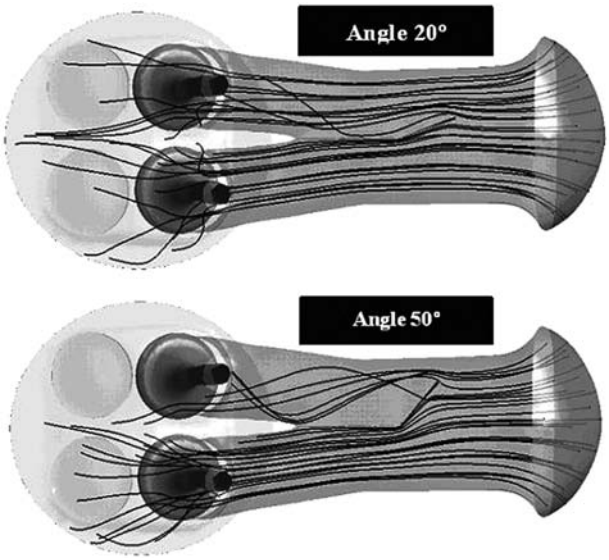

Fig. 22 Streamlines showing the effect produced by introducing the swirl deflector at two positions

head, like volumetric performance and angular momentum production (tumble and swirl). Based on these tests the following conclusions were reached.

1. Experimental and numerical results show the existence of a cooperative effect when both valves are equally opened, clearly improving the volumetric efficiency.
2. The tumble bench proposed showed significant advantages over other current designs. As the tumble loss rate along the lateral duct decays linearly, this allows estimation of the in-cylinder tumble by measuring at two different positions.
3. CFD allows the tumble fall at mean valve lift to be captured. This phenomenon was also observed experimentally. This effect is related to changes in the vortex pattern below valves, produced while valves are opening. Although this effect is strongly observed during a steady test, its occurrence in dynamic situations is

negligible because of the speed of the process. This means that the steady test should be used only at high valve lifts.

4. Valve timings (delay between valves or a valve completely closed) seem to offer useful techniques for controlling the in-cylinder charge motion. The production of swirl in a four-valve-per-cylinder engine requires high valve delays; otherwise swirl becomes negligible after the mean valve lift. However, for partial load, swirl motion is more attractive because of its inherent stability until the spark ignition.
5. The use of flow deflectors is a suitable option to control the in-cylinder charge motion. The proposed deflectors allowed an increase in tumble or swirl generation for high load or for partial load requirements, respectively. Although deflectors had a negative impact on the volumetric efficiency, they are useful for enhancing the turbulence of the charge at partial load, increasing the fuel burning rate and improving combustion efficiency.

ACKNOWLEDGEMENT

The authors would like to thank CONICET and ANPCyT (grants PICT Lambda 12-14573/2003, PME 209/2003). They are also grateful to Fia, Argentina for donating the engine to carry out this work. Finally, thanks are owed to Miguel Ramos, who helped the authors perform the experimental tests, and Nicolás Schiliuk, who contributed to improving this work.

REFERENCES

1 **Huang, R. F., Lin, K. H., Yeh, C. N.,** and **Lan, J.** In-cylinder tumble flows and performance of a motorcycle engine with circular and elliptic intake ports. *Expl Fluids*, 2009, **46**, 165–179.

2 **Lee, K., Bae, C.,** and **Kang, K.** The effects of tumble and swirl flows on flame propagation in a four-valve S.I. engine. *Appl. Thermal Engng*, 2007, **27**, 2122–2130.

3 **Ramajo, D.** and **Nigro, N.** In-cylinder flow CFD analysis of a 4-valve spark ignition engine. Comparison between steady and dynamic tests. *J. Engng Gas Turbines and Power*, 2010, **132**(5), 121–131.

4 **Mariani, F.** and **Cavalletti, M.** Dependence of flow characteristics of a high performance S.I. engine intake system on test pressure and tumble generation conditions – part 2: numerical analysis. SAE paper 2004-01-1531, 2004.

5 **Grimaldi, C., Battistone, M.,** and **Uccellani, G.** Dependence of flow characteristics of a high performance S.I. engine intake system on test pressure and tumble generation conditions – part 1: experimental analysis. SAE paper 2004-01-1530, 2004.

6 **Grimaldi, C., Battistone, M.,** and **Postrioti, L.** Flow characterization of a high performance S.I. engine intake system – part 1: experimental analysis. SAE paper 2003-01-0623, 2003.

7 **Mattarelli, E.** Comparison between two combustion chambers for a motorcycle racing engine. SAE paper 2000-01-1894, 2000.

8 **Ramajo, D.** *Simulación computacional de los procesos fluido-dinámicos en el interior de motores de combustión interna*. PhD Thesis, Universidad Nacional del Litoral, Argentina, 2008, available from http://www.cimec.org.ar/ojs/index.php/cimec-repo/article/view/1384.

9 **Mahmood, Z., Chen, A., Yianneskis, M.,** and **Ganti, G.** On the structure of steady flow through dual-intake engine ports. *Int. J. Numer. Methods Fluids*, 1996, **23**, 1085–1109.

10 **Gosman, A. D.** State of the art of multi-dimensional modeling of engine reacting flows. *Oil Gas Sci. Technol.*, 1999, **54**(2), 149–159.

11 **Lopez, E., Nigro, N.,** and **Storti, M.** Simultaneous untangling and smoothing of moving and fixed grids. *Int. J. Numer. Methods Engng*, 2008, **77**(7), 994–1019.

12 **Bailly, O., Buchou, C., Floch, A.,** and **Sainsaulieu, L.** Simulation of the intake and compression strokes of a motored 4-valve SI engine with a finite element code. *Oil Gas Sci. Technol.*, 1999, **54**(2), 161–168.

13 **Li, L., Tao, J., Wang, Y., Su, Y.,** and **Xiao, M.** Effects of intake valve closing timing on gasoline engine performance and emissions. SAE paper 2001-01-3564, 2001.

14 **Mahrous, A., Wysznski, M., Xu, H.,** and **Tsolakis, A.** A CFD investigation into the effects of intake valves events on airflow characteristics in a motored 4-valve engine cylinder with negative valve overlapping. In Proceedings of the ICE2007 SAE Conference, 07-NAPLES-74, Italy, September 2007, SAE paper 2007-24-0032.

15 **Ramajo, D., Zanotti, A.,** and **Nigro, N.** Assessment of a zero-dimensional model of tumble in four-valve high performance engine. *Int. J. Numer. Methods Heat and Fluid Flow*, 2007, **17**(8), 770–787.

16 **Xu, H.** Some critical technical issues on the steady flow testing of cylinder heads. SAE paper 2001-01-1308, 2001.

17 **Grimaldi, C., Battistone, M.,** and **Mariani, F.** Experimental and numerical analysis of charge motion characteristics depending on intake valves actuation strategies. SAE paper 2005-01-0242, 2005.

18 **Jeon, C., Chang, Y., Cho, K. B.,** and **Kang, K. Y.** Effects of intake ports on in-cylinder flow and lean combustion in a 4-valve engine. SAE paper 981048, 1998.

19 **Aleiferis, P. G., Taylor, A. M. K. P., Ishii, K.,** and **Urata, Y.** The nature of early flame development in a lean-burn stratified-charge spark-ignition engine. *Combust. Flame*, 2004, **136**, 283–302.
20 **Tan, Z.** and **Reitz, R. D.** An ignition and combustion model based on the level-set method for spark ignition engine multidimensional modeling. *Combust. Flame*, 2006, **145**, 1–15.
21 **Lee, D.** and **Heywood, J. B.** Effects of charge motion control during cold start of SI engines. SAE paper 2006-01-3399, 2006.
22 **Wilson, N., Watkins, A.,** and **Dopson, C.** Asymmetric valve strategies and their effect on combustion. SAE paper 930821, 1993.
23 **Geiger, J., Grigo, M., Lang, O., Wolters, P.,** and **Hupperich, P.** Direct injection gasoline engines – combustion and design. SAE paper 199-01-0170, 1999.
24 **Peng, Z.–J.** and **Jia, M.** An investigation and evaluation of variable-valve-timing and variable-valve-actuation strategies in a diesel homogeneous charge compression ignition engine using three-dimensional computational fluid dynamics. *Proc. IMechE, Part D: J. Automobile Engineering*, 2008, **222**(6), 1047–1064. DOI: 10.1243/09544070JAUTO760.
25 **Yun, J.-E.** New evaluation index for bulk motion of in-cylinder flow through intake port system in cylinder head (II). *Int. J. Veh. Des.*, 2002, **30**(4), 279–290.
26 **Li, Y., Liu, S., Shi, S-X., Feng, M.,** and **Sui, X.** An investigation of in-cylinder tumbling motion in a four-valve spark ignition engine. *Proc. IMechE, Part D: J. Automobile Engineering*, 2001, **215**(2), 273–284. DOI: 10.1243/0954407011525511.
27 **Heywood, J. B.** *Internal combustion engines fundamentals*, 1988 (McGraw Hill, New York).
28 **Fontana, G., Galloni, E., Jannelli, E.,** and **Palmaccio, R.** Influence of the intake system design on a small spark-ignition engine performance. A theoretical analysis. SAE paper 2003-01-3134, 2003.
29 **Fontana, G., Galloni, E., Palmaccio, R.,** and **Torella, E.** The influence of variable timing on the combustion process of a small spark-ignition engine. SAE paper 2006-01-0445, 2006.
30 **He, Y., Selamet, A., Reese, R., Vick, R.,** and **Amer, A.** Impact of tumble on combustion in SI engines: correlation between flow and engine experiments. SAE paper 2007-01-4003, 2007.
31 **He, Y.** *Effect of intake primary runner blockages on combustion characteristics and emissions in spark ignition engines*. PhD Thesis, University of Ohio, USA, 2007.

APPENDIX

Notation

Bo	cylinder bore
C_D	discharge coefficient
C_f	flow coefficient
C_1	model constant ($C_1 = 1.44$)
C_2	model constant ($C_2 = 1.92$)
C_μ	model constant ($C_\mu = 0.09$)
G	turbulence production term
k	turbulent kinetic energy
l	cylinder height
P	static pressure
$\boldsymbol{U}$	Reynolds average velocity
V_t	tangential velocity
ε	turbulence dissipation rate
μ_t	turbulent viscosity
ρ	air density
σ_ε	model constant ($C_\sigma = 1.3$)
σ_κ	model constant ($C_k = 1.0$)
τ	shear stress tensor
ϕ	external volumetric momentum source
ω	rotational velocity

Acronyms

ACT	tumble bench adaptor
CFD	computational fluid dynamics
MFR	mass flowrate
SD	swirl deflector
SM	swirl meter
TD	tumble deflector